

Quantitative Predictions of the Interfacial Tensions of Liquid–Liquid Interfaces through Atomistic and Coarse Grained Models

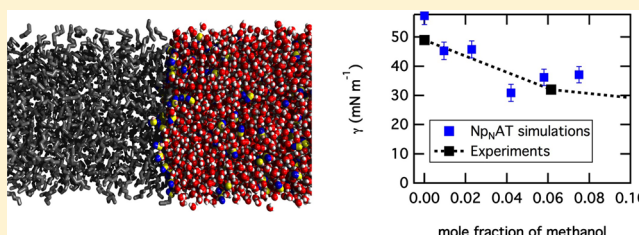
Jean-Claude Neyt,^{†,‡} Aurélie Wender,[‡] Véronique Lachet,[‡] Aziz Ghoufi,[§] and Patrice Malfreyt^{*,†}

[†]Clermont Université, Université Blaise Pascal, Institut de Chimie de Clermont-Ferrand, BP 10448, F-63000 Clermont-Ferrand, France

[‡]IFP Energies nouvelles, 1-4 avenue de Bois Préau, 92852 Reuil-Malmaison, France

[§]Institut Physique de Rennes, Université Rennes 1, 35042 Rennes, France

ABSTRACT: We report molecular simulations of oil–water liquid–liquid interfaces by using atomistic and coarse grained (CG) MARTINI force fields. We also apply the electronic continuum (EC) model to the MARTINI force field for the calculation of the interfacial tension of oil/water-salt systems. In a first step, we propose to calculate the interfacial tensions using thermodynamic and mechanical definitions of hydrocarbon–water interfacial systems modified by the addition of salts and alcohol. We also establish here the order of magnitude of the long-range corrections to the interfacial tension in fluid–fluid interfaces. Whereas the atomistic models are able to reproduce quantitatively the interfacial tension and the coexisting densities of oil–water systems, the coarse-description shows some deviations in the prediction of the interfacial tensions. Nevertheless, the physical features of these liquid–liquid interfaces are well-captured by this CG description. The CG force field offers then a very challenging alternative that will require however a more developed calibration of the parameters on the basis of liquid–liquid properties.



1. INTRODUCTION

The first two-phase molecular simulation was launched on a liquid–vapor interface of a Lennard-Jones (LJ) fluid¹ 40 years ago. After a scan of the literature, we observe that studies on the surface of tension of LJ fluid^{2,3} are still published in 2013, demonstrating that the molecular simulation of liquid–vapor interfaces remains an active field of research by continuing to address a number of fundamental methodological issues. It is now well-established that the calculation of the surface tension of liquid–vapor interfaces depends on a number of factors such as the finite size effects,^{4–7} the range of interactions,^{8–11} the truncation effects,^{8,12–14} the mechanical and thermodynamic definitions used for the surface tension calculation,^{13,15,16} and the long-range corrections to be applied to the surface tension.^{10,12,13,16–18} In spite of these methodological aspects that impact the results of surface tension, the two-phase simulations of liquid–vapor interfaces are now able to reproduce the temperature dependence of the surface tension of various organic liquids,^{10,12,13,19–27} water,^{28–30} acid gases,^{16,29,31–33} and incondensable gases.³³ The molecular simulation of the liquid–vapor interfaces of multicomponent mixtures is much less widespread. Indeed, few molecular simulations^{34–37} report the pressure dependence of the surface tension of mixtures.^{34–38}

The molecular simulation of liquid–liquid is even more challenging due to the system sizes required to stabilize the liquid phases and the interfacial region. Whereas most simulations of liquid–liquid interfaces^{39–43} have been developed to study mainly the structure of the interface in

terms of density distributions and specific molecular orientations, much fewer simulations have been devoted to a quantitative reproduction of the interfacial tension.^{44–50} Actually, such liquid–liquid interfaces raise many methodological questions concerning the statistical ensemble, the expressions used for the calculation of the long-range correction, the system-size dependence of the interfacial tension, and the respect of the mechanical equilibrium of these liquid–liquid planar interfaces.

Many chemical, physical, and biological processes such as micelle and membrane formation, protein folding, drug delivery, oil extraction, and chemical separation involve the presence of a water–oil interface. As a result, the interfacial tension of water–hydrocarbon systems^{51–54} is a key property for understanding the intermolecular forces at the interfacial region. Another interesting issue concerns the change of the interfacial tension upon addition of small organic solutes⁵⁵ and inorganic ions.⁵¹ Whereas molecular simulation offers a promising alternative to theoretical⁵⁶ and experimental approaches by combining a molecular description of the interface region with an energetic characterization of the different bulk and interfacial phases, a question arises on the most adapted level of description of the matter to predict accurately the interfacial tension of these complex water–oil systems with a reasonable computational effort. Indeed, some

Received: January 23, 2014

Published: April 16, 2014

coarse-grained (CG) models^{57–59} have already been successfully applied to the study of alkane/water interfaces.

In this paper, we propose to model the *n*-octane/water liquid–liquid interface by using both atomistic and coarse-grained models. The accuracy and the convergence of the interfacial tension will be evaluated through the different mechanical and thermodynamic definitions of the surface tension. As far as we know, this work applies for the first time the test-area (TA)¹⁵ and KBZ¹⁶ approaches on the calculation of the interfacial tension of a liquid–liquid interface. We also consider explicitly the calculation of the long-range corrections to the interfacial tension by rigorous expressions that have been successfully applied to the liquid–vapor of a multicomponent mixture.^{37,38} From a methodological viewpoint, this calculation of the long-range correction within the different definitions is very interesting due to the fact that this contribution has never been considered in the past in the calculation of the interfacial tension of liquid–liquid interfaces due to the difficulty of calculating it. We definitively establish the order of magnitude of this tail contribution in the interfacial tension of oil/water interfaces. Indeed, this tail correction to the surface tension can represent at least 25% to the surface tension for liquid–vapor systems^{10,12} interacting through Lennard-Jones interactions. We have also observed that these long-range corrections can never be neglected in systems for which the electrostatic interactions were predominant.²⁹ We extend this work by comparing the atomistic and CG descriptions on the *n*-octane/water interface upon the addition of NaCl salt. We investigate the ability of the force fields to reproduce the salt concentration dependence of the interfacial tension. We also take the route of applying the electronic continuum (EC) model^{60,61} to the MARTINI force field in order to model implicitly the polarization effects. Such an implicit modeling of the polarization contribution has already been carried out with atomistic force fields.⁶² To complete this study, we will test the ability of the atomistic models to reproduce quantitatively the change of the interfacial tension with respect to the addition of a small surfactant.

The paper is then organized as follows. Section 2 describes the different atomistic and coarse-grained potentials used. The calculation of the surface tension is described in section 3 within the different definitions. Section 4 discusses the main results in terms of interfacial tension and microscopic insights of the different types of interfaces. Section 5 contains our conclusions and gives some outlooks for the modeling of complex liquid–liquid interfaces.

2. SIMULATION DETAILS

2.1. Potential Models. The atomistic and coarse-grained potentials used here are based upon the assumption that the two-body additive terms are predominant and that the remaining nonadditive many-body interactions (especially the three-body term) can be considered as captured by the effective pairwise additive potentials of the atomistic and coarse-grained force fields.

2.1.1. Atomistic Description. The *n*-pentane and *n*-octane molecules are described using the TraPPE-UA united atom model⁶³ where CH₃ and CH₂ groups are represented with a single center of force. The methanol is also modeled by the TraPPE-UA force field⁶⁴ where the CH₃ group is represented by a united atom and the oxygen and hydrogen atoms by explicit atoms. The water is modeled using the TIP4P/2005 description,⁶⁵ whereas the sodium and chloride ions are

modeled using the parameters of the OPLS force field.^{66–69} We opt for these potentials because it has been established by different studies that they perform very well in the reproduction of the temperature dependence of the surface tension of liquid–vapor interfaces of alkanes,²² water,²⁹ and salts.^{62,70}

The total configurational energy *U* sums the intramolecular and intermolecular energy contributions. Because the water molecule is considered as rigid, $U_{\text{INTRA}} = 0$. For the *n*-alkane molecules, the intramolecular interactions include contributions from the bending energy, torsion energy, and nonbonded interactions, whereas the length of the C–C bond is fixed and equal to 1.54 Å (see Table 1). The expressions for the bending

Table 1. Details of the Atomistic Force Fields for the Description of Water, *n*-Alkanes, and Salt Ions

| TIP4P/2005 water model ⁶⁵ | | | |
|--|----------------------|--------------------------|-----------|
| | σ (Å) | ϵ/k_B (K) | q (e) |
| O | 3.1589 | 93.2 | 0 |
| H | 0 | 0 | 0.5564 |
| M | 0 | 0 | −1.1128 |
| distance OH (Å) | | 0.9572 | |
| angle H–O–H (deg) | | 104.52 | |
| distance OM (Å) | | 0.1546 | |
| OPLS model ^{66–69} | | | |
| | σ (Å) | ϵ/k_B (K) | q (e) |
| Na ⁺ | 1.897 44 | 808.74 | +1 |
| Cl [−] | 4.417 24 | 59.27 | −1 |
| TraPPE-UA model - alkane ⁶³ | | | |
| | σ (Å) | ϵ/k_B (K) | q (e) |
| CH ₃ | 3.75 | 98 | 0 |
| CH ₂ | 3.95 | 46 | 0 |
| distance CH _x –CH _x (Å) | 1.54 | | |
| angle CH _x –CH _x –CH _x (deg) | $\theta_0 = 114.0$ | $k_\theta/k_B = 62500$ K | |
| torsion CH _x –CH ₂ –CH ₂ –CH _x (deg) | $C_0/k_B = 0$ K | $C_1/k_B = 335.03$ K | |
| | $C_2/k_B = -68.19$ K | $C_4/k_B = 791.32$ K | |
| TraPPE-UA model - alcohol ⁶⁴ | | | |
| | σ (Å) | ϵ/k_B (K) | q (e) |
| CH ₃ | 3.75 | 98 | 0.265 |
| O | 3.02 | 93 | −0.700 |
| H | | | 0.435 |
| distance CH ₃ –O (Å) | 1.43 | | |
| distance O–H (Å) | 0.945 | | |
| angle CH ₃ –O–H (deg) | $\theta_0 = 108.5$ | $k_\theta/k_B = 55400$ K | |

potential energy and the torsion potential energy can be found elsewhere.⁷¹ For the methanol, Table 1 reports the parameters of the force field along with the partial charges: the distance CH₃–O is maintained to 1.43 Å. The intramolecular nonbonded interactions occur between groups separated by more than three bonds and were computed using the same Lennard-Jones 6–12 potential as intermolecular interactions.

The intermolecular interactions are composed of repulsion–dispersion and electrostatic contributions that are represented by Lennard-Jones and Coulombic potentials, respectively. The parameters of the repulsion–dispersion interactions are given in Table 1. The LJ parameters for the interactions between unlike sites were calculated using the Lorentz–Berthelot combining

rules. The electrostatic interactions were calculated using the Ewald sum method.^{31,72–74}

2.1.2. MARTINI Force Field. The coarse-grained model consists of reducing the degrees of freedom by coarsening the model. Each interaction center (called bead) may represent then few atoms. There is no unique way to construct coarse-grained (CG) models of molecules.^{75,76} We take the route of using here the MARTINI force field.^{57,58,77,78} In this model, the *n*-octane molecule is modeled by using two beads connected by a weak harmonic potential defined by

$$U_{\text{bond}}(r_{ij}) = \frac{1}{2} k_{\text{bond}} (r_{ij} - r_0)^2 \quad (1)$$

where r_{ij} is the distance between two beads i and j and r_0 is the equilibrium distance between these two beads. The values of k_{bond} and r_0 are given in Table 2.

Table 2. Details of the Coarse Grained MARTINI Force Field for the Description of Water, *n*-Alkanes, and Salt Ions

| water MARTINI model ⁷⁷ | | | |
|---|----------------|---|--------------------|
| | σ (Å) | ϵ/k_B (K) | q (e) |
| W | 4.7 | 481.1 | 0 |
| WP | 0 | 0 | 0.46 |
| WM | 0 | 0 | −0.46 |
| distance W–WP, W–WM (Å) | 1.4 | | |
| angle WP–W–WM (rad) | $\theta_0 = 0$ | $k_\theta/k_B = 505.2$ K rad ^{−2} | |
| alkane and salt MARTINI models ⁵⁸ | | | |
| | σ (Å) | ϵ/k_B (K) | q (e) |
| C4 | 4.7 | 421.0 | 0 |
| distance C4–C4 (Å) | $r_0 = 4.7$ | $k_b/k_B = 1503$ K Å ^{−2} | |
| Na ⁺ | 4.7 | 421.0 | +1 |
| Cl [−] | 4.7 | 421.0 | −1 |
| EC model ^{60,61} | | | |
| | σ (Å) | ϵ/k_B (K) | q (e) |
| Na ⁺ | 4.7 | 421.0 | +1.6 |
| Cl [−] | 4.7 | 421.0 | −1.6 |
| matrix of nonbonded LJ interactions ⁵⁸ | | | |
| site | site | σ (Å) | ϵ/k_B (K) |
| C4 | C4 | 4.7 | 421.0 |
| W | W | 4.7 | 481.1 |
| Na | Na | 4.7 | 421.0 |
| Cl | Cl | 4.7 | 421.0 |
| C4 | W | 4.7 | 228.5 |
| C4 | Na | 4.7 | 276.6 |
| C4 | Cl | 4.7 | 276.6 |
| W | Na | 4.7 | 601.4 |
| W | Cl | 4.7 | 601.4 |
| Na | Cl | 4.7 | 481.1 |

The electrostatic version of the MARTINI model of water⁷⁷ considers three particles W, WP, and WM along with five parameters. The central W particle is connected to WP and WM particles by constrained bonds of a length of 1.4 Å and by a harmonic angle potential function with θ_0 and k_θ parameters. The values of these parameters are given in Table 2. The CG MARTINI water model represents four water molecules. The reader is redirected to ref 77 for a comprehensive description of the model. Intramolecular interactions between nonbonded atoms occur between atoms separated by more than one bond

and are modeled using the following Lennard-Jones and electrostatic potentials.

In addition to these intramolecular interactions, the total intermolecular interaction sums the repulsion-dispersion and electrostatic interactions as

$$U_{\text{INTER}} = U_{\text{LJ}} + U_{\text{ELEC}} \quad (2)$$

where U_{LJ} is given by

$$U_{\text{LJ}} = \sum_{i=1}^{N-1} \sum_{j>i}^N \sum_{a=1}^{n_i} \sum_{b=1}^{n_j} 4\epsilon_{ab} \left[\left(\frac{\sigma_{ab}}{r_{iagb}} \right)^{12} - \left(\frac{\sigma_{ab}}{r_{iagb}} \right)^6 \right] \quad (3)$$

where r_{iagb} is the distance between the force center of particle a in molecule i and force center of particle b in molecule j , ϵ_{ab} is the energy parameter of the interaction, and σ_{ab} is the Lennard-Jones core diameter. n_i and n_j are the number of force centers in the molecules i and j , respectively. N is the total number of water, alkanes, and salt molecules. The LJ parameters ϵ_{ab} and σ_{ab} for the different types of beads are given in Table 2.

The electrostatic interactions were calculated using the Coulombic potential as

$$U_{\text{ELEC}} = \sum_{i=1}^{N-1} \sum_{j>i}^N \sum_{a=1}^{n_i} \sum_{b=1}^{n_j} \frac{q_{ia} q_{jb}}{4\pi\epsilon_0\epsilon_r r_{iagb}} \quad (4)$$

where q_{ia} is the charge of particle a in molecule i . ϵ_0 is the permittivity in a vacuum, and ϵ_r is the relative dielectric constant. For the electrostatic version of the water MARTINI model,⁷⁷ ϵ_r was taken equal to 2.5. Both LJ and Coulombic potential functions are then modified by cubic spline functions^{12,78,79} with cutoff radii r_s and r_c equal to 9 and 12 Å, respectively. To be in line with the standard MARTINI force field,⁵⁸ all the CG beads have the same mass, $m = 72$ amu, corresponding to four water molecules.

Recently, the electronic continuum (EC) model^{60,61} has been proposed to consider electronic polarization into nonpolarizable models. The dipole moment of the water MARTINI model⁷⁷ is $\mu^{\text{eff}} = 4.9$ D compared to an experimental dipole moment of the liquid phase⁸⁰ of $\mu = 3.1$ D. As a result, the partial charges of the coarse grained water model can be interpreted as scaled effective charges. The unscaled dipole moment of the MARTINI model should be equal to $\mu = \mu^{\text{eff}} \sqrt{\epsilon_c} = 3.1$ D assuming $\epsilon_c = 0.40$. The EC methodology consists then of scaling all the electrostatic interactions by the factor $1/\epsilon_c$. It results then that the effective charges of the ions are then scaled by $\pm 1/\sqrt{\epsilon_c}$. The values of the charges with the EC model are given in Table 2.

3. SURFACE TENSION

During this past decade, there has been an active development of theoretical approaches for the calculation of the surface tension. These approaches led to operational expressions that have been mainly applied to liquid–vapor interfaces. The most commonly used methods^{15,81–85} for the surface tension calculation are based upon the mechanical route definition. The first explicit form (γ_{KB}) developed by Kirkwood and Buff⁸² expresses the components of the pressure tensor as a function of the derivative of the intermolecular potential. The definition of Irving and Kirkwood⁸³ (γ_{IK}) is based upon the notion of the force across a unit area and allows one to describe the interfacial region in terms of local pressure components. A method based upon the thermodynamic definition of the

surface tension (γ_{TA}) has been established by Gloor et al.¹⁵ and consists of perturbing the cross-sectional area of the system containing the interface. We present the different operational expressions of the surface tension with the corresponding expressions of their long-range corrections. Let us consider a system of N molecules with two planar liquid–liquid surfaces lying in the x, y plane where z represents then the direction normal to the surface.

3.1. Kirkwood–Buff Relation (KB). The molecular surface tension γ_{KB} was first introduced by Kirkwood and Buff⁸² and makes use of the molecular virial expression to give the following relationship:

$$\gamma_{KB} = \frac{1}{2} \langle p_N - p_T \rangle L_z \quad (5)$$

where p_N and p_T are the normal and tangential components of the pressure, respectively. L_z is the dimension of the simulation cell along the z axis. The normal component p_N is equal to p_{zz} whereas the tangential component p_T is given by $1/2(p_{xx} + p_{yy})$.

The element $\alpha\beta$ of the molecular pressure tensor is defined as

$$p_{\alpha\beta} = \rho k_B T \mathbf{I} + \frac{1}{V} \left\langle \sum_{i=1}^{N-1} \sum_{j>i}^N (\mathbf{r}_{ij})_{\alpha} (\mathbf{F}_{ij})_{\beta} \right\rangle \quad (6)$$

where \mathbf{I} is the unit tensor, T is the input temperature, and $\rho = N/V$ is the number density. α and β represent x, y , or z directions. \mathbf{r}_{ij} is the vector between the centers of mass of molecules i and j . \mathbf{F}_{ij} in eq 6 is the intermolecular force between molecules i and j and is expressed as the sum of all the site–site forces acting between these two molecules.

$$\mathbf{F}_{ij} = \sum_{a=1}^{n_i} \sum_{b=1}^{n_j} (\mathbf{f}_{iajb}) = - \sum_{a=1}^{n_i} \sum_{b=1}^{n_j} \frac{\mathbf{r}_{iajb}}{r_{iajb}} \frac{dU(r_{iajb})}{dr_{iajb}} \quad (7)$$

The definition of the molecular pressure tensor given in eq 6 is only valid for additive potentials. In the case of electrostatic interactions calculated using the Ewald summation method, the contribution to the potential in the real space is pairwise-additive, whereas the contribution in the reciprocal space is not. It means that eq 6 is not applicable for the contribution in the reciprocal space. A comprehensive description of the dispersion-repulsion and electrostatic energy contributions to the pressure calculation can be found in ref 38. The long-range correction to the surface tension will be calculated by using the expression established in the KBZ approach.

3.2. Irving and Kirkwood Definition (IK). The method of Irving and Kirkwood (IK)⁸³ expresses the surface tension from the local components of the pressure tensor

$$\gamma_{IK} = \frac{1}{2} \int_{-L_z/2}^{L_z/2} (p_N(z_k) - p_T(z_k)) dz_k \quad (8)$$

where $p_N(z_k)$ and $p_T(z_k)$ are the normal and tangential components of the pressure tensor along the normal to the surface, respectively. The L_z dimension of the box is divided into slabs of width δz . z_k is the position of the slab k along z . The method of Irving and Kirkwood⁸³ (IK) is based upon the notion of the force across a unit area. The pressure tensor is then written as a sum of a kinetic term and a potential term resulting from the intermolecular forces. Whereas the first term is well-defined, the potential term is subjected to arbitrariness because there is no unique way to determine which intermolecular forces contribute to the stress across dA .

There are many ways of choosing the contour joining two interacting particles. Irving and Kirkwood⁸³ have chosen as a contour the straight line between the two particles. Other choices are possible and result from the lack of uniqueness in the definition of the microscopic stress tensor. The components of the pressure tensor^{81,84,85} in the Irving and Kirkwood definition are expressed by

$$p_{\alpha\beta}(z_k) = \langle \rho(z_k) \rangle k_B T \mathbf{I} + \frac{1}{A} \left\langle \sum_{i=1}^{N-1} \sum_{j>i}^N (\mathbf{r}_{ij})_{\alpha} (\mathbf{F}_{ij})_{\beta} \frac{1}{|z_{ij}|} \theta \left(\frac{z_k - z_i}{z_{ij}} \right) \theta \left(\frac{z_j - z_k}{z_{ij}} \right) \right\rangle \quad (9)$$

where $\theta(x)$ is the unit step function defined by $\theta(x) = 0$ when $x < 0$ and $\theta(x) = 1$ when $x \geq 0$. A is the surface area normal to the z axis. $\rho(z_k)$ is the total number density calculated in the slab k . The distance z_{ij} between two molecular centers of mass is divided into N_s slabs of thickness δz . Following Irving and Kirkwood, the molecules i and j give a local contribution to the pressure tensor in a given slab if the line joining the centers-of-mass of molecules i and j crosses, starts, or finishes in the slab. Each slab has $1/N_s$ of the total contribution from the i – j interaction. The different electrostatic contributions to the pressure tensor can be found elsewhere, refs 34, 35, for completeness.

The LRC part of the surface tension is then calculated using the LRC parts of the pressure tensor that have been derived by Guo and Lu.⁸⁶

$$\gamma_{IK,LRC}(z_k) = \frac{\pi}{2} \rho(z_k) \frac{V_s}{A} \sum_{i=1}^{N_C} \sum_{j=1}^{N_C} x_i(z_k) \int_{r_c}^{\infty} dr \int_{-r}^r d\Delta z [\rho_j(z) - \rho_j(z_k)] \frac{dU_{ij,LJ}(r)}{dr} [r^2 - 3(\Delta z)^2] \quad (10)$$

where $\rho_j(z_k)$ is the density number of the species j in the slab k . $x_i(z_k)$ is the mole fraction of molecular species i in the slab k . N_C is the number of molecular types in the system; here, $N_C = 2, 3$, or 4 . Δz is defined as the difference $z - z_k$ and varies between $-r$ and r . r_c is the cutoff radius, $U_{ij,LJ}(r)$ is the intermolecular Lennard-Jones energy with r being the distance between the two centers of mass of molecules of species i and j .

$$U_{ij,LJ}(r) = \sum_a \sum_b \epsilon_{ab} \left[\left(\frac{\sigma_{ab}}{r} \right)^{12} - \left(\frac{\sigma_{ab}}{r} \right)^6 \right] \quad (11)$$

The LRC to the surface tension is obtained by summing up all the contributions to the local values of each bin and dividing the result by 2. In eq 10, V_s is the volume of the slab k .

3.3. Test-Area Method (TA). The test-area method¹⁵ (TA) is based upon a thermodynamic route and expresses the surface tension as a change in the free energy⁸⁷ for an infinitesimal change in the surface area. This change in the area is performed throughout a perturbation process for which the perturbed system (state ^{$A+\Delta A$}) is obtained from an infinitesimal change ΔA of the area A of the reference system. The box dimensions ($L_x^{(A+\Delta A)}$, $L_y^{(A+\Delta A)}$, $L_z^{(A+\Delta A)}$) in the perturbed systems are changed using the following transformations: $L_x^{(A+\Delta A)} = L_x^{(A)} (1$

$+ \xi)^{1/2}$, $L_y^{(A+\Delta A)} = L_y^{(A)}(1 + \xi)^{1/2}$, $L_z^{(A+\Delta A)} = L_z^{(A)}/(1 + \xi)^{1/2}$ where $\xi \rightarrow 0$. The area $(A + \Delta A)$ of the perturbed state thus equals to $L_x^{(A)}L_y^{(A)}(1 + \xi)$, and ΔA is equal to $L_x^{(A)}L_y^{(A)}\xi$. The operational expression for the calculation of γ within the TA method is

$$\gamma_{TA} = \sum_k \lim_{\xi \rightarrow 0} -\frac{k_B T}{\Delta A} \ln \left\langle \exp \left(-\frac{(U^{(A+\Delta A)}(z_k, \mathbf{r}^N) - U^{(A)}(z_k, \mathbf{r}^N))}{k_B T} \right) \right\rangle_{k,A} \quad (12)$$

$\langle \dots \rangle_{k,A}$ indicates that the average is carried out over the reference state and the k slabs. $U^{(A+\Delta A)}(z_k, \mathbf{r}^N)$ and $U^{(A)}(z_k, \mathbf{r}^N)$ are the configurational energies of the slab k in the perturbed and reference states. These energy contributions sum the Lennard-Jones and electrostatic interactions. The expression given in eq 12 is obtained by assuming that the energy of the slab at position z_k is uncorrelated with that of the slab at z_{k+1} . This approximation was validated in a previous paper.¹³ For the calculation of the energy, we adopt the definition of Ladd and Woodcock⁸⁸ and choose to assign in the slab centered on z_k two energy contributions: one contribution due to the energy between the molecules within the slab and a second contribution due to the energy of the molecules within the slab with those outside the slab. The energy of the slab at the position z_k is defined as

$$U(z_k) = \sum_{i=1}^N H_k(z_i) \left[\left(\frac{1}{2} \sum_{j \neq i}^N \sum_a^{n_i} \sum_b^{n_j} u_{LJ}(r_{iajb}) + u_{ELEC,R}(r_{iajb}) \right) + \left(\sum_a^{n_i} u_{ELEC,H}(r_{ia}) \right) \right] \quad (13)$$

where $u_{ELEC,R}(r_{iajb})$ and $u_{ELEC,H}(r_{ia})$ correspond to the real space and reciprocal contributions of the Ewald summation technique. $H_k(z_i)$ is a top-hat function with functional values of

$$\begin{cases} H_k(z_i) = 1 & \text{for } z_k - \frac{\delta z}{2} < z_i < z_k + \frac{\delta z}{2} \\ H_k(z_i) = 0 & \text{otherwise} \end{cases} \quad (14)$$

The total LRC contribution of the surface tension with the TA approach is expressed as a function of the long-range correction energy. The tail correction of the surface tension within the test-area formalism is approximated by

$$\begin{aligned} \gamma_{TA,LRC} &= \sum_k \lim_{\xi \rightarrow 0} -\frac{k_B T}{\Delta A_\xi} \\ &\times \ln \left\langle \exp \left(-\frac{(u_{LRC}^{(2),(A+\Delta A)}(z'_k) - (u_{LRC}^{(2),(A)}(z_k)))}{k_B T} \right) \right\rangle_0 \\ &= \sum_k \gamma_{LRC}(z_k) \end{aligned}$$

where

$$u_{LRC}^{(2)}(z_k) = \pi \rho(z_k) V_s \sum_{i=1}^{N_c} \sum_{j=1}^{N_c} x_i(z_k) \int_{r_c}^{\infty} dr \int_{-r}^r d\Delta z [\rho_j(z) - \rho_j(z_k)] r U_{ij,LJ}(r) \quad (15)$$

Further details concerning this expression can be found in ref 13. The calculation of the surface tension was carried out in the direct ($\gamma_{TA,D}$) and reverse ($\gamma_{TA,I}$) directions. The calculation in the direct direction involves an increase of the surface area $(A + \Delta A)$, whereas a decrease of the surface area $(A - \Delta A)$ is performed in the reverse path. The ensemble average was carried out over the configurations of the reference system, whereas the configurations of the perturbed system are only virtual. Thermodynamic consistency requires that the surface tension in the direct and reverse directions must be equal in magnitude and opposite in sign. This is satisfied when the configuration space of the perturbed system matches that of the reference system. This requirement implies the use of an appropriate value of ξ . We have found that $\xi = 5 \times 10^{-4}$ represented a reasonable value^{7,16,22,23,29,32} for this calculation.

3.4. Local Expression of the Surface Tension from the Virial Route (KBZ). The local version of the surface tension based upon the KB expression has been established elsewhere.¹⁶ The working expression was obtained from the derivative of the potential with respect to the surface and was referred as the KBZ method in this paper. The expression of the surface tension within the KBZ approach in the Np_NAT statistical ensemble can be written as

$$\begin{aligned} \gamma_{KBZ} &= \left\langle \frac{\partial U}{\partial A} \right\rangle_0 = \sum_k \left\langle \frac{\partial U_{z_k}}{\partial A} \right\rangle_0 = \sum_k \gamma_{KBZ}(z_k) \\ &= \sum_k (\gamma_{KBZ}^{LJ}(z_k) + \gamma_{KBZ}^{ELEC}(z_k)) \end{aligned} \quad (16)$$

The analytical expressions of $\gamma_{KBZ}^{LJ}(z_k)$ and $\gamma_{KBZ}^{ELEC}(z_k)$ can be found in previous papers.^{34,35} The local versions $\gamma_{TA}(z_k)$ and $\gamma_{KBZ}(z_k)$ can be compared to the standard local version $\gamma_{IK}(z_k)$ and allow for checking the features of the profile of the surface tension calculated from the new approach TA and the well-known approach of Kirkwood and Buff. In fact, the local version of the surface tension using the KBZ approach can be considered as the local version of the Kirkwood and Buff definition. The values of surface tension calculated from the local expressions are identical to those calculated from the macroscopic expressions of γ_{KBZ} and γ_{TA} within a maximum deviation of 0.01%.

The working local LRC expression for the surface tension within the Np_NAT ensemble using the KBZ definition is given by the following equation

$$\begin{aligned} \gamma_{KBZ,LRC}(z_k) &= \pi \rho(z_k) \frac{V_s}{2A} \sum_{i=1}^{N_c} \sum_{j=1}^{N_c} x_i(z_k) \int_{r_c}^{\infty} dr \\ &\int_{-r}^r d\Delta z [\rho_j(z) - \rho_j(z_k)] \left(\frac{r^2 - 3(\Delta z)^2}{r} \right) \\ &\times \left(U_{ij,LJ}(r) + r \frac{\partial U_{ij,LJ}(r)}{\partial r} \right) \end{aligned} \quad (17)$$

3.5. Molecular Dynamics Simulations. 3.5.1. Atomistic Simulations. The equations of motion were solved using the

Berendsen⁸⁹ algorithm with a time step of 2 fs. MD simulations were performed with the DL_POLY code⁹⁰ in the Np_NAT ensemble at $T = 298$ K and 0.1 MPa. The volume of the system was changed by varying the longitudinal dimension L_z of the box in each cycle while keeping the interfacial area A constant. Because the longitudinal dimension of the box changes during the course of the simulation, the profiles along the direction normal to the surface are plotted as a function of the reduced z_k/L_z property. The initial simulation box was a rectangular parallelepipedic box of dimensions $L_x L_y L_z$ ($L_x = L_y = 50$ Å). The number of water molecules was fixed to 6200 and the number of alkanes molecules to 1400. The number of salt ions was changed from 110 to 330 to respect 1 and 3 M ion concentrations. The number of methanol molecules was varied from 0 to 600 corresponding to molar fractions ranging from 0 to 7.5%. A typical configuration of n -octane-water + salt ions is shown in Figure 1. Periodic boundary conditions were applied

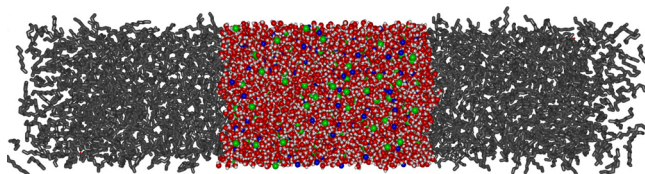


Figure 1. An equilibrium configuration of n -octane/water + NaCl salt at a salt molality of 3 m at 298 K and 0.1 MPa resulting from a two-phase atomistic simulation.

in the three directions. Standard deviations of the ensemble averages were calculated by breaking the production runs into block averages. The calculated number of block averages was adjusted in order to allow the convergence of the surface tension within each block.²³ The cutoff radius r_c was set to 12 Å. The systems were equilibrated for 2 ns followed by a production phase of 10 ns.

3.5.2. Coarse Grained Simulations. The n -octane/water system was modeled using 2863 CG water molecules and 1186 CG alkane molecules with box dimensions of $L_x = L_y = 54$ Å. The equations of motion were solved using the Berendsen⁸⁹ algorithm with a time step of 10 fs over an acquisition period of 10 ns. The equilibration period was also 10 ns. The thermodynamic conditions are identical to those used in atomistic simulations.

4. RESULTS AND DISCUSSIONS

The molecular densities of the oil and water phases are shown in Figure 2 for the atomistic model as a function of the reduced z^* coordinate. Figure 2a shows two well-developed phases and well-defined interfaces without any oscillation in the octane density profile close to the water surface. The profiles of water and octane molecules are very flat over a region of approximately 60 Å (corresponding to 0.3 in reduced units). We also observe a monotonic decrease of the alkane density profile in the interfacial region, and $\rho(z^*)$ vanishes at the vicinity of the water bulk region. Panel b of Figure 2 compares the density profiles of atomistic and CG models and represents the experimental bulk density values of pure water and pure n -octane at 298 K and 1 bar.⁹¹ The agreement between simulated densities using atomistic models and experiments is excellent with deviations of 0.6% and 0.1% for n -octane and water, respectively. The quality of the prediction underlines the performance of the Np_NAT statistical ensemble and the

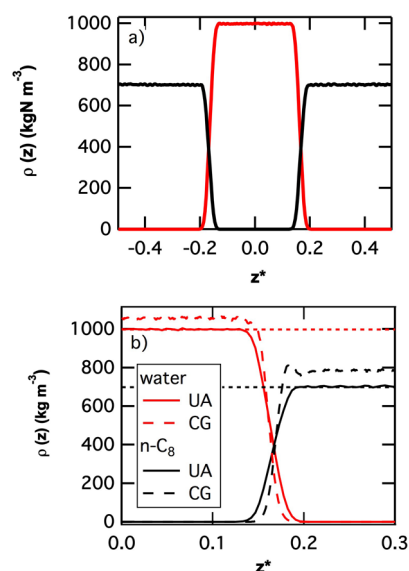


Figure 2. (a) Molecular density profiles of the n -octane/water liquid-liquid interface at 298 K under 0.1 MPa as a function of the reduced z position. (b) Zoom of the density profiles in one interfacial region with the values of the experimental liquid densities of water and n -octane under the same thermodynamic conditions.

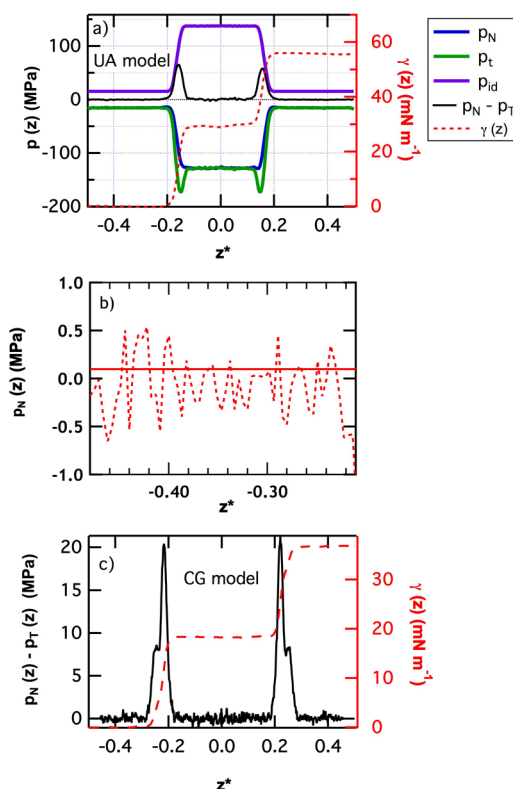


Figure 3. (a) Decomposition of the profiles of the normal and tangential pressure components into the kinetic and potential parts for the n -octane/water interface. The profiles of the difference between the normal and tangential components and of its integral are also shown in the case of the atomistic UA force field. (b) Profile of the normal pressure component calculated in the bulk alkane phase. The solid line shows the target pressure of 0.1 MPa. (c) The profiles of $p_N - p_T$ and $\gamma(z)$ calculated with the CG MARTINI model.

atomistic force field to reproduce the coexisting densities of two liquid phases. We observe larger deviations with the CG

Table 3. Interfacial Tensions (mN m^{-1}) of Different *n*-Octane/Water Interfaces Using Atomistic and Coarse-Grained Descriptions^a

| | γ_{KB} | | γ_{IK} | | γ_{TA} | | γ_{KBZ} | | $\langle \gamma \rangle$ | $\gamma_{\text{exp.}}$ | |
|----------|--|--------------------|-----------------------|--------------------|-----------------------|-------------------|-----------------------|-------------------|--------------------------|------------------------|----------------|
| | γ_{LRC} | γ | γ_{LRC} | γ | γ_{LRC} | γ | γ_{LRC} | γ | | | |
| | <i>n</i> -octane/water | | | | | | | | | | |
| | UA model | | | | | | | | | | |
| | 0.0 ₁ | 55.6 ₁₂ | 0.1 ₁ | 55.6 ₁₂ | 0.2 ₁ | 57.0 ₅ | 0.0 ₁ | 55.8 ₅ | 56.1 ₁₂ | 52.5 | |
| | MARTINI model | | | | | | | | | | |
| | | 39.1 ₈ | | 36.9 ₈ | | 39.2 ₈ | | 39.2 ₈ | 38.0 ₈ | 52.5 | |
| | <i>n</i> -octane/water + Na ⁺ + Cl [−] | | | | | | | | | | |
| | UA model | | | | | | | | | | |
| | <i>m</i> | | | | | | | | | $\Delta\gamma$ | |
| | 1 | 0.0 ₁ | 56.3 ₁₂ | 0.1 ₁ | 56.3 ₁₂ | 0.2 ₁ | 57.7 ₅ | 0.1 ₁ | 56.5 ₅ | 56.8 ₁₂ | 0.7 |
| | 3 | 0.0 ₁ | 61.9 ₂₂ | 0.1 ₁ | 61.9 ₂₂ | 0.2 ₁ | 63.0 ₂₂ | 0.1 ₁ | 62.2 ₂₂ | 62.2 ₂₂ | 6.1 |
| <i>m</i> | MARTINI model | | | | | | | | | | $\Delta\gamma$ |
| 0.6 | | 39.5 ₈ | | 37.3 ₉ | | 39.5 ₈ | | 39.5 ₅ | 38.9 ₈ | 0.9 | |
| 1.2 | | 40.2 ₈ | | 38.1 ₉ | | 40.2 ₈ | | 40.2 ₅ | 39.7 ₈ | 1.7 | |
| 1.8 | | 41.9 ₈ | | 39.8 ₉ | | 41.9 ₈ | | 41.9 ₅ | 41.4 ₈ | 3.4 | |
| 2.3 | | 45.0 ₈ | | 43.8 ₉ | | 45.0 ₈ | | 45.0 ₅ | 44.7 ₈ | 6.7 | |
| 2.8 | | 46.7 ₈ | | 44.5 ₉ | | 46.7 ₈ | | 46.7 ₅ | 46.1 ₈ | 8.1 | |
| <i>m</i> | MARTINI + EC model | | | | | | | | | | $\Delta\gamma$ |
| 0.6 | | 40.7 ₇ | | 38.7 ₅ | | 40.7 ₇ | | 40.7 ₆ | 40.2 ₈ | 2.2 | |
| 1.2 | | 41.5 ₈ | | 38.5 ₆ | | 41.5 ₈ | | 41.5 ₆ | 40.8 ₈ | 2.8 | |
| 1.8 | | 42.1 ₈ | | 40.9 ₆ | | 42.1 ₈ | | 42.1 ₈ | 41.8 ₈ | 3.8 | |
| 2.3 | | 43.7 ₈ | | 41.8 ₅ | | 43.7 ₈ | | 43.7 ₈ | 43.2 ₈ | 5.2 | |
| 2.8 | | 44.5 ₇ | | 42.5 ₆ | | 44.5 ₇ | | 44.5 ₇ | 44.0 ₇ | 6.0 | |

^aThe subscripts give the accuracy of the last decimal(s), i.e., 56.1₁₂ means 56.1 ± 1.2 . The experimental interfacial tension of the water–octane interface is taken from ref 52. $\Delta\gamma = \gamma_{\text{octane-water+salt}} - \gamma_{\text{octane-water}}$. *m* corresponds to the salt molality.

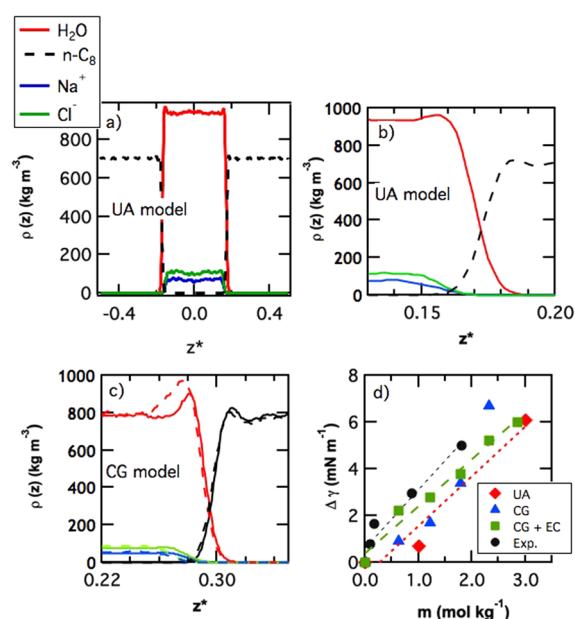


Figure 4. (a) Molecular density profiles of the octane and water molecules as well as those of the salt ions at a molality of 3.0 mol kg^{−1}. Zoom of the density profiles in the interfacial region in the case of (b) the atomistic model and (c) the GC MARTINI model at a molality of 2.8 mol kg^{−1}. The solid and dotted lines show the profiles of the MARTINI force field and the MARTINI + EC model, respectively. (d) Dependence of the relative interfacial tension as a function of the molality of salt solutions for the different models. The experimental data are taken from ref 51, and the dotted lines represent the estimated regression lines.

model of about 6% for the water density and 12% for the alkane density. In addition, Figure 2b shows a slight narrower interface

with the CG description and an oscillation in the density profile of *n*-octane close to the interface. This oscillation, which does not appear with the atomistic models, is not present when the atomistic definition is used for calculating the density profile. Such an oscillation has already been observed in a previous study⁴¹ with atomistic models. The origin of this oscillation can come from size effects, the statistical ensemble, the force field used, and the definition used for the calculation of $\rho(z)$. We will see thereafter that this oscillation also impacts the profiles of the pressure components along the normal to the interface.

Figure 3a shows the kinetic and potential parts of normal and tangential components of the pressure tensor calculated with the atomistic force field as a function of z^* . The kinetic part, which can be expressed by the ideal-gas contribution $\rho(z)k_{\text{B}}T$, has the same shape as the total molecular density profile. The potential part is identical for the normal and tangential pressure components in the bulk alkane and water phases, whereas the potential contribution of the tangential pressure component exhibits a negative peak at the interface. The resulting difference between the normal and tangential components shows two positive peaks at the interfacial regions. The integration of the $p_{\text{N}} - p_{\text{T}}$ profile gives the $\gamma(z)$ curve that establishes flat portions in the bulk phases indicating that only the interfacial regions contribute to the value of the interfacial tension. These profiles also indicate that the contribution to the interfacial tension from both interfaces is the same. All these profiles show mechanical features that are expected from an equilibrium planar liquid–liquid interface. These local properties are key elements that allow a definitive conclusion on the quality of the statistics and a rejection of any problem of convergence in the calculation of the interfacial tension. In addition, the profile of the normal component p_{N} in the alkane phase (see Figure 3b) shows that the simulated pressure matches very well with the target pressure of 0.1 MPa. Figure

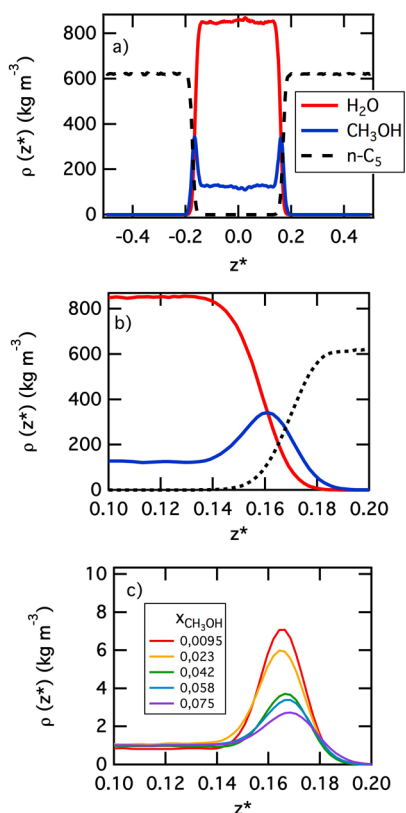


Figure 5. Molecular density profiles of the *n*-pentane/water liquid–liquid interfaces modified by the addition of methanol. (a) Total density profiles of water, pentane, and methanol molecules for a mole fraction of methanol of 0.0075. (b) Zoom of the different density profiles at the interfacial region for the same concentration of methanol. (c) Normalized density profiles of the methanol with respect to the concentration of methanol in the bulk water phase as a function of the amount of methanol.

3c shows the profiles of $p_N - p_T$ and of its integral $\gamma(z)$ calculated using the CG MARTINI model. As expected, $\gamma(z)$ is constant in the bulk phases and the contribution from both interfaces is the same. Very interestingly, we observe in the $p_N - p_T$ profile a shoulder in the peaks toward the alkane phase. This shoulder takes its origin in the oscillation found in the density profile that leads to an additional negative contribution of the tangential pressure component. This was already observed with the MARTINI force field on the hexadecane/water interface.⁹²

We now turn our attention to the prediction of the interfacial tension of the *n*-octane/water interface. Although a certain number of studies^{44,46,93,94} report the calculation of the interfacial tension of *n*-alkane/water liquid–liquid interfaces, it is not always easy to understand the differences between the calculated surface tensions and to rationalize the deviations between simulations and experiments. The scattering of the simulated values of surface tension finds its origin in the various methodologies used that differ in the definitions of the surface tension and of its long-range corrections, size-effects, force field, simulation time, and statistical ensemble. Here, after a careful check of the methodology, we use four different approaches for the calculation of interfacial tensions. We also take care to calculate rigorously the long-range corrections to the interfacial tension that have been ignored in most simulations. The values of the interfacial tensions calculated using the different

definitions and their long-range corrections are reported in Table 3. From a methodological side, we observe that the TA method, which uses a perturbation formalism, performs very well in the case of a liquid–liquid interface. Additionally, the values of the long-range corrections to the interfacial tensions are negligible for all the definitions used here. That explains why in the past they were neglected in most simulations of liquid–liquid interfaces. However, such long-range corrections can represent contributions ranging from 10% to 40% of the total surface tension of liquid–vapor interface depending on the temperature and nature of interactions involved.⁹⁵ The four definitions give interfacial tension values within 1.4 mN m^{-1} (2.5%) for the atomistic models and within 2.4 mN m^{-1} (5.8%) for the CG models. When we average the interface tensions over the four approaches for the atomistic model, we obtain a simulated value that deviates by less than 7% from experiments. It represents then a good prediction for this property. The calculation of the interfacial tension by using the CG MARTINI force field is a little less predictive, the deviation reaches 27% from experiments, and it is in the same order of magnitude as what was obtained from some atomistic simulations.^{44,46,93,94} It means that the CG MARTINI force field must be calibrated on a more developed set of thermodynamic properties for a better reproduction of the interfacial tension. With the MARTINI force field, the long-range corrections are rigorously zero, because the force and energy functions¹² are modified by switching functions that make the potential and its derivative zero at the cutoff value.

We now focus on the *n*-octane/water interface modified by the addition of NaCl salt. We propose here to check the dependence of the interfacial tension on the salt concentration. We will use standard nonpolarizable atomistic models because we have shown in a recent paper⁷⁰ that only the nonpolarizable models are able to reproduce the linear increase of the surface tension of liquid–vapor interface of aqueous NaCl solutions with respect to salt concentrations. For this reason, we retain the TIP4P/2005 water model and the OPLS force field for the ions. For the atomistic model, we simulate only two molalities (1 and 3 mol kg^{-1}). Figure 4a shows the different molecular density profiles of water and *n*-octane along with those of the Na^+ and Cl^- ions at 3 mol kg^{-1} . Panel a of this figure exhibits well-developed regions of bulk phases with ions which are homogeneously distributed in the water phase. By focusing on the interfacial region, Figure 4b shows clearly that the ions do not populate the interface region which remains devoid of ions. The presence of the ions seems to slightly perturb the interface region compared to that of the binary *n*-octane/water system by creating a very small oscillation in $\rho(z)$ at the water and alkane surfaces. A typical equilibrium configuration of this interface is given in Figure 7a that allows one to check that the ions do not sample the interfacial region. Figure 4c represents the density profiles of this interfacial system modeled using the CG model of the MARTINI force field. The same features are then reproduced by the CG model: no accumulation of ions in the interfacial region and small oscillations in $\rho(z)$ at the water and alkane surfaces. In the case of the water liquid phase, we observe an underestimation of the liquid density. We add for comparison the profiles calculated using the CG + EC model. We do not observe any significant differences in the density profiles when the charges of the ions are scaled. Only a slight increase in $\rho(z)$ at the water surface is noted. The numerical values of surface tensions are reported in Table 3 for each definition and model. We also report the relative interfacial

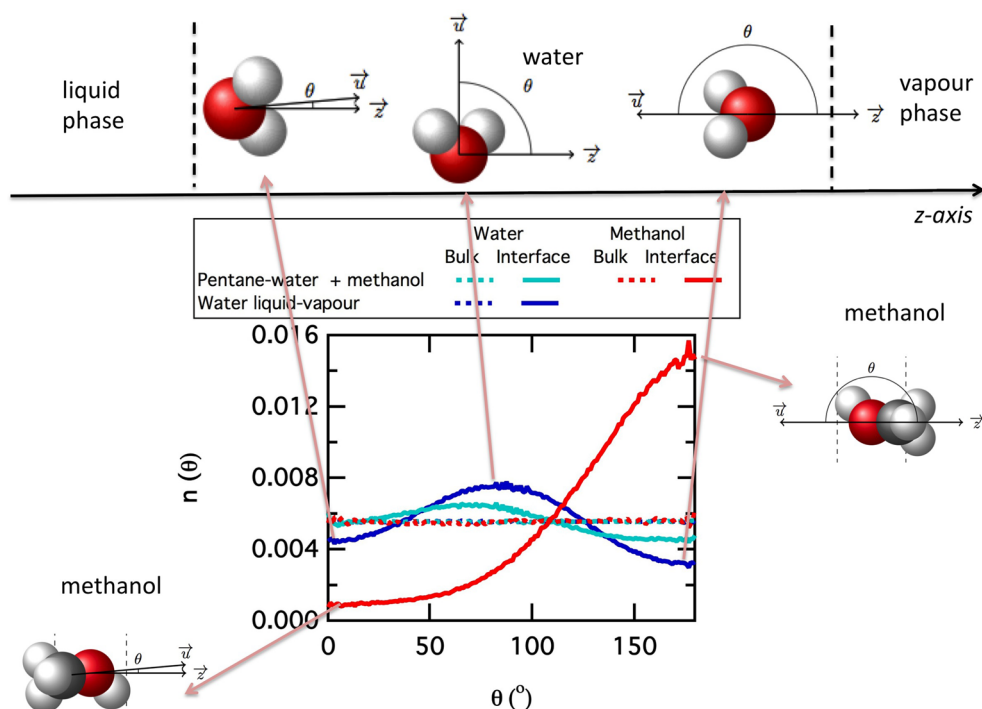


Figure 6. Distribution of the θ angle between the molecular dipole vector of water or methanol and the vector normal to the surface in different liquid–liquid interfaces. The *n*-octane/water + salt corresponds to a molality of 3 mol kg^{−1} and the *n*-pentane/water + methanol to a methanol mole fraction of 0.0075.

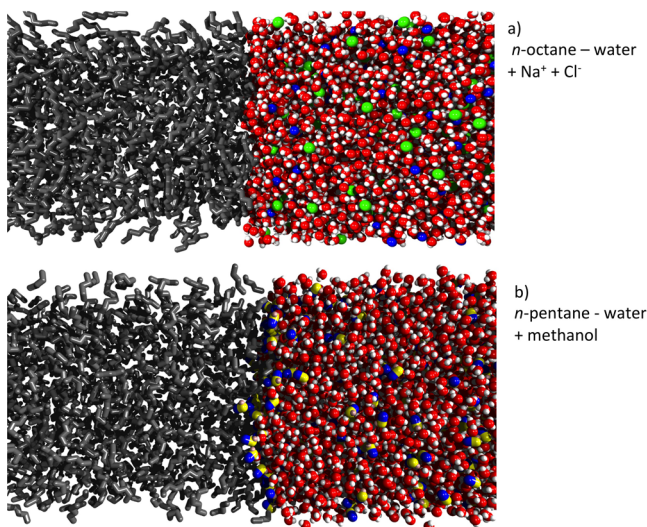


Figure 7. Different typical equilibrium configurations of liquid–liquid interfacial systems. (a) *n*-octane/water + NaCl at 3m and (b) *n*-pentane/water at 0.075 mole fraction of methanol.

tension $\Delta\gamma$ defined as the interfacial tension of the (*n*-octane/water + NaCl) system minus that of the (*n*-octane/water) system. This property allows one to check the ability of the model to reproduce the relative increase of interfacial tension upon the addition of salt. First, the order of magnitude of the long-range corrections for the atomistic model remains very small leading to a maximum contribution of 0.3% to the total surface tension. The simulated relative interfacial tensions $\Delta\gamma$ are represented in panel d of Figure 4 along with the available experimental data.⁵¹ These curves show that the effect of the salinity on the relative interfacial tension is qualitatively reproduced from the atomistic and CG models. Since the

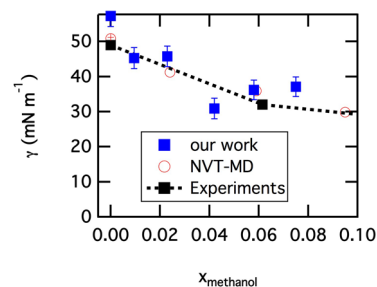


Figure 8. Interfacial tension γ (mN m^{−1}) of the *n*-pentane/water liquid–liquid interface modified by the addition of methanol for different mole fractions of alcohol. For comparison, experimental interfacial tensions are represented⁵⁵ along with NVT-MD simulations.⁴⁶

absolute value of the *n*-octane/water system is better reproduced by atomistic models, we observe in Table 3 that the interfacial tension of the *n*-octane/water + salt system is quantitatively predicted using atomistic models. For the CG models, the interfacial tension of this system presents some deviations from experiments, but interestingly, the effect of adding salt is satisfactorily reproduced on the relative interfacial tension in comparison to experiments. For the CG + EC model, we obtain a slope ($d\Delta\gamma/dm$) of 2 ± 0.1 mN m^{−1} mol^{−1} kg, whereas the corresponding experimental value for the liquid–vapor interfaces of aqueous salt solutions is 1.9.⁹⁶ A more quantitative prediction calls for further developments of the CG models in order to reproduce both the surface tension of pure liquid–vapor interface of water and the interfacial tension of liquid–liquid oil–water systems.

We complete this study by the modeling of the liquid–liquid interface of the *n*-pentane/water system modified by the addition of an alcohol molecule that can be considered as a

Table 4. Interfacial Tensions (mN m^{-1}) of the *n*-Pentane/Water + Methanol Interfaces Calculated with UA Models As a Function of the Mole Fraction of Methanol (x)^a

| x | γ_{KB} | | γ_{IK} | | γ_{TA} | | γ_{KBZ} | | $\langle \gamma \rangle$ | $\gamma_{\text{exp.}}$ |
|------------------------------------|-----------------------|--------------------|-----------------------|--------------------|-----------------------|--------------------|-----------------------|--------------------|--------------------------|------------------------|
| | γ_{LRC} | γ | γ_{LRC} | γ | γ_{LRC} | γ | γ_{LRC} | γ | | |
| <i>n</i> -pentane/water + methanol | | | | | | | | | | |
| 0.0 | 0.1 ₁ | 57.7 ₃₀ | 0.1 ₁ | 57.7 ₃₀ | 0.2 ₁ | 58.2 ₃₀ | 0.1 ₁ | 55.5 ₃₀ | 57.3 ₃₀ | 49.0 |
| 0.0095 | 0.1 ₁ | 45.2 ₃₀ | 0.1 ₁ | 46.0 ₃₀ | 0.2 ₁ | 46.4 ₃₀ | 0.1 ₁ | 43.9 ₃₀ | 45.4 ₃₀ | 46.2 |
| 0.023 | 0.1 ₁ | 46.3 ₂₉ | 0.1 ₁ | 46.2 ₂₉ | 0.2 ₁ | 46.6 ₂₉ | 0.1 ₁ | 44.1 ₂₉ | 45.8 ₂₉ | 42.6 |
| 0.042 | 0.1 ₁ | 31.3 ₂₉ | 0.1 ₁ | 31.3 ₂₉ | 0.2 ₁ | 31.7 ₂₉ | 0.1 ₁ | 29.5 ₂₉ | 30.9 ₂₉ | 37.4 |
| 0.058 | 0.1 ₁ | 36.5 ₂₈ | 0.1 ₁ | 36.5 ₂₈ | 0.2 ₁ | 37.0 ₂₈ | 0.1 ₁ | 34.7 ₂₈ | 36.2 ₂₈ | 33.0 |
| 0.075 | 0.1 ₁ | 37.7 ₂₈ | 0.1 ₁ | 37.5 ₂₈ | 0.2 ₁ | 37.9 ₂₈ | 0.1 ₁ | 35.6 ₂₈ | 37.1 ₂₈ | 31.0 |

^aThe subscripts give the accuracy of the last decimal(s), i.e., 57.3₃₀ means 57.3 ± 3.0 . The experimental interfacial tensions are taken from ref 55.

small surfactant. This system allows one to check the quantitative prediction of atomistic models on the effect of a small surfactant on the interfacial tension and the resulting changes in the structure of the interfacial region. We then perform various atomistic simulations at different mole fractions of methanol in the water phase. Figure 5 shows the molecular density profiles of water, *n*-pentane, and methanol molecules. When we compare these density profiles with those of previous simulations⁴⁶ calculated in NVT molecular simulations, we clearly observe that our molecular simulations in the *Np_NAT* simulations give very well converged density profiles without any oscillation in both water and alkane phases. The molecular density profiles of the methanol show that this alcohol is homogeneously distributed in the water phase with enhancements of density in the interfacial region. Panel b of Figure 5 focuses on the interfacial region. The density profile of the methanol overlaps the density profiles of the water and *n*-pentane molecules. In this region, the methanol molecules point their dipole moments to the water phase as can be seen in Figure 6. The methanol molecule in the interfacial region bridges the gap between the water and alkane phases and as a result reduces the hydrophobic barrier between the two phases. Panel c of Figure 5 confirms this point by showing the density profiles of methanol as a function of the mole fraction of alcohol. This figure shows that the enhancement of density with respect to that of the bulk methanol phase decreases with increasing amount of methanol. It shows the propensity of methanol to concentrate at the oil–water interface even at small concentrations as expected from a surfactant. The orientational structure of the water and methanol molecules in the interfacial and bulk regions is illustrated in Figure 6 through the distribution of the angle between the water dipole vector and the vector normal to the surface. Figure 6 shows there is a broad range of possible orientations for water in the interfacial region, whereas this angle distribution is flat in an isotropic bulk environment. The angle distribution of methanol shows significant differences between the bulk and interfacial regions. Indeed, in the interfacial region, this distribution shows that angles of 180° are favored, indicating most methanol molecules point their dipole moment toward the water phase: the hydroxyl groups are located in the water phase and the methyl groups in the oil phase in line with the behavior of a surfactant (see Figure 7b for an equilibrium configuration of the oil–water + methanol system). To quantify the effect of adding methanol, we report in Figure 8 the interfacial tension as a function of the mole fraction of methanol. Very interestingly, we observe that the atomistic simulations are able to qualitatively reproduce the decrease of the interfacial tension with the concentration of methanol. We also report the

interfacial tensions⁴⁶ calculated from a previous work in the constant-NVT ensemble that does not allow one to predict the coexisting densities of the phases in contact. Over the [0.0,0.06] range of mole fraction, the experimental interface tension⁵⁵ decreases by 35%, whereas the molecular simulations in the *Np_NAT* also predict 35% of the decrease. Table 4 reports the experimental and simulated interfacial tensions at different mole fractions. Even if the absolute simulated interfacial tensions can deviate a little from experiments with a maximum deviation of 25% from experiments⁵⁵ over the range of methanol concentrations, the relative decrease of the interface tension is well-reproduced.

5. CONCLUSIONS

Different methodological aspects have been investigated related to the molecular simulation of the liquid–liquid interfaces of hydrocarbon–water systems. We aimed to definitively conclude on the ability of the *Np_NAT* statistical ensemble and the atomistic united atom models to be predictive on both the coexisting densities and interfacial tensions. Such simulations have required addressing a number of fundamental questions concerning the order of magnitude of the long-range corrections of interfacial tensions in liquid–liquid systems, the resulting mechanical equilibrium of such interfacial systems, and the ability of the different thermodynamic and mechanical definitions of the interfacial tension to give reasonable values in comparison to experiments. We complete the methodological part of this work by applying coarse-grained models on these liquid–liquid interfaces and by extending the methodology of the calculation of the interfacial tension from atomistic simulations to CG simulations. The use of CG models represents a first step toward more quantitative predictions of the interfacial tension of liquid–liquid interfaces. We have also studied the impact of the electronic continuum model on the quality of the prediction of the interfacial tension of oil/water–salt systems.

The predictive aspect of the atomistic models has been evaluated on hydrocarbon–water liquid–liquid interfaces modified on the one hand by the addition of salt and the other hand by the addition of a small surfactant. In all cases, we can conclude that the use of the atomistic models offers a quantitative prediction of the interfacial tension of these complex interfaces upon the addition of salt and alcohol with however an important computational effort. The use of a coarse grained description of the interactions remains an attractive approach with a genuine computational gain (10 times faster than atomistic simulations). The agreement with experiments remains qualitative, but the systems presented here are quite complicated regarding the variety and the type of interactions.

However, these CG models have demonstrated their ability to reproduce the effect of salinity on the increase of the relative interfacial tension of an alkane/water system. Additionally, the structural features of the liquid–liquid interfaces are well-reproduced by these CG models in line with those described by the atomistic force field. By using the same strategy as that used for the atomistic force field, these CG models could be calibrated over more developed databases. As a result, these CG models open the way to offering more quantitative predictions of interfacial systems.

AUTHOR INFORMATION

Corresponding Author

*E-mail: Patrice.Malfreyt@univ-bpclermont.fr.

Notes

The authors declare no competing financial interest.

REFERENCES

- (1) Liu, K. S. Phase separation of Lennard-Jones systems: A film in equilibrium with vapor. *J. Chem. Phys.* **1974**, *60*, 4226–4230.
- (2) Martinez-Valencia, A.; Gonzalez-Melchor, M.; Orea, P.; Lopez-Lemus, J. Liquid-vapour interface varying the softness and range of the interaction potential. *Mol. Simul.* **2013**, *39*, 64–71.
- (3) Mgue, J. M.; Pineiro, M. M.; Blas, F. J. Influence of the long-range corrections on the interfacial properties of molecular models using Monte Carlo simulation. *J. Chem. Phys.* **2013**, *138*, 034707.
- (4) Orea, P.; Lopez-Lemus, J.; Alejandre, J. Oscillatory surface tension due to finite-size effects. *J. Chem. Phys.* **2005**, *123*, 114702.
- (5) Gonzalez-Melchor, M.; Orea, P.; Lopez-Lemus, J.; Bresme, F.; Alejandre, J. Stress anisotropy induced by periodic boundary conditions. *J. Chem. Phys.* **2005**, *122*, 094503.
- (6) Errington, J. R.; Kofke, D. A. Calculation of surface tension via area sampling. *J. Chem. Phys.* **2007**, *127*, 174709.
- (7) Biscay, F.; Ghoufi, A.; Goujon, F.; Lachet, V.; Malfreyt, P. Calculation of the surface tension from Monte Carlo simulations: Does the model impact on the finite-size effects? *J. Chem. Phys.* **2009**, *130*, 184710.
- (8) Trokhymchuk, A.; Alejandre, J. Computer simulations of liquid/vapor interface in Lennard-Jones fluids: Some questions and answers. *J. Chem. Phys.* **1999**, *111*, 8510–8523.
- (9) Lopez-Lemus, J.; Alejandre, J. Thermodynamic and transport properties of simple fluids using lattice sums: bulk phases and liquid-vapour interface. *Mol. Phys.* **2002**, *100*, 2983–2992.
- (10) Goujon, F.; Malfreyt, P.; Boutin, A.; Fuchs, A. H. Direct Monte Carlo simulations of the equilibrium properties of n-pentane liquid–vapor interface. *J. Chem. Phys.* **2002**, *116*, 8106–8117.
- (11) Grosfils, P.; Lutsko, J. F. Dependence of the liquid-vapor surface tension on the range of interaction: A test of the law of corresponding states. *J. Chem. Phys.* **2009**, *130*, 054703.
- (12) Goujon, F.; Malfreyt, P.; Simon, J. M.; Boutin, A.; Rousseau, B.; Fuchs, A. H. Monte Carlo versus molecular dynamics simulations in heterogeneous systems: An application to the n-pentane liquid-vapor interface. *J. Chem. Phys.* **2004**, *121*, 12559–12571.
- (13) Ibergay, C.; Ghoufi, A.; Goujon, F.; Ungerer, P.; Boutin, A.; Rousseau, B.; Malfreyt, P. Molecular simulations of the n-alkane liquid-vapor interface: Interfacial properties and their long range corrections. *Phys. Rev. E* **2007**, *75*, 051602.
- (14) Goujon, F.; Bonal, C.; Malfreyt, P. Calculation of the long-range interactions for interfacial properties. *Mol. Simul.* **2009**, *35*, 538–546.
- (15) Gloor, G. J.; Jackson, G.; Blas, F. J.; de Miguel, E. Test-area simulation method for the direct determination of the interfacial tension of systems with continuous or discontinuous potentials. *J. Chem. Phys.* **2005**, *123*, 134703.
- (16) Ghoufi, A.; Goujon, F.; Lachet, V.; Malfreyt, P. Expressions for local contributions to the surface tension from the virial route. *Phys. Rev. E* **2008**, *77*, 031601.
- (17) Guo, M.; Lu, B. C. Y. Long range corrections to thermodynamic properties of inhomogeneous systems with planar interfaces. *J. Chem. Phys.* **1997**, *106*, 3688–3695.
- (18) Shen, V. K.; Mountain, R. D.; Errington, J. R. Comparative Study of the Effect of Tail Corrections on Surface Tension Determined by Molecular Simulation. *J. Phys. Chem. B* **2007**, *111*, 6198–6207.
- (19) Goujon, F.; Malfreyt, P.; Boutin, A.; Fuchs, A. H. Vapour-liquid phase equilibria of n-alkanes by direct Monte Carlo simulations. *Mol. Simul.* **2001**, *27*, 99–114.
- (20) Janeczek, J.; Krienke, H.; Schmeer, G. Inhomogeneous Monte Carlo simulation of the vapor-liquid equilibrium of benzene between 300 and 530 K. *Condens. Matter Phys.* **2007**, *10*, 415–423.
- (21) Nieto-Draghi, C.; Bonnaud, P.; Ungerer, P. Anisotropic united atom model including the electrostatic interactions of methylbenzenes. I. Thermodynamic and structural properties. *J. Phys. Chem. C* **2007**, *111*, 15686–15699.
- (22) Biscay, F.; Ghoufi, A.; Goujon, F.; Lachet, V.; Malfreyt, P. Surface Tensions of linear and branched alkanes from Monte Carlo simulations using the anisotropic united atom model. *J. Phys. Chem. B* **2008**, *112*, 13885–13897.
- (23) Biscay, F.; Ghoufi, A.; Lachet, V.; Malfreyt, P. Calculation of the surface tension of cyclic and aromatic hydrocarbons from Monte Carlo simulations using an anisotropic united atom model (AUA). *Phys. Chem. Chem. Phys.* **2009**, *111*, 6132–6147.
- (24) Biscay, F.; Ghoufi, A.; Malfreyt, P. Surface tension of water-alcohol mixtures from Monte Carlo simulations. *J. Chem. Phys.* **2011**, *134*, 044709.
- (25) Biscay, F.; Ghoufi, A.; Lachet, V.; Malfreyt, P. Prediction of the Surface Tension of the Liquid-Vapor Interface of Alcohols from Monte Carlo Simulations. *J. Phys. Chem. C* **2011**, *115*, 8670–8683.
- (26) Ferrando, N.; Lachet, V.; Pérez-Pellitero, J.; Mackie, A. D.; Malfreyt, P.; Boutin, A. A transferable force field to predict phase equilibria and surface tension of ethers and glycol ethers. *J. Phys. Chem. B* **2011**, *115*, 10654–10664.
- (27) Zubillaga, R. A.; Labastida, A.; Cruz, B.; Martinez, J. C.; Sanchez, E.; Alejandre, J. Surface Tension of Organic Liquids Using the OPLS/AA Force Field. *J. Chem. Theory Comput.* **2013**, *9*, 1611–1615.
- (28) Vega, C.; de Miguel, E. Surface tension of the most popular models of water by using the test-area simulation method. *J. Chem. Phys.* **2007**, *126*, 154707.
- (29) Ghoufi, A.; Goujon, F.; Lachet, V.; Malfreyt, P. Surface tension of water and acid gases from Monte Carlo simulations. *J. Chem. Phys.* **2008**, *128*, 154716.
- (30) Ghoufi, A.; Malfreyt, P. Mesoscale modeling of the water liquid-vapor interface: A surface tension calculation. *Phys. Rev. E* **2011**, *83*, 051601.
- (31) Alejandre, J.; Tildesley, D. J.; Chapela, G. A. Molecular dynamics simulation of the orthobaric densities and surface tension of water. *J. Chem. Phys.* **1995**, *102*, 4574–4573.
- (32) Ghoufi, A.; Goujon, F.; Lachet, V.; Malfreyt, P. Multiple histogram reweighting method for the surface tension calculation. *J. Chem. Phys.* **2008**, *128*, 154718.
- (33) Neyt, J. C.; Wender, A.; Lachet, V.; Malfreyt, P. Prediction of the Temperature Dependence of the Surface Tension of SO₂, N₂, O₂, and Ar by Monte Carlo Molecular Simulations. *J. Phys. Chem. B* **2011**, *115*, 9421–9430.
- (34) Biscay, F.; Ghoufi, A.; Lachet, V.; Malfreyt, P. Monte Carlo calculation of the methane-water interfacial tension at high pressures. *J. Chem. Phys.* **2009**, *131*, 124707.
- (35) Biscay, F.; Ghoufi, A.; Lachet, V.; Malfreyt, P. Monte Carlo Simulations of the Pressure Dependence of the Water-Acid Gas Interfacial Tensions. *J. Phys. Chem. B* **2009**, *113*, 14277–14290.
- (36) Miqueu, C.; Miquez, J. M.; Pineiro, M.; Lafitte, T.; Mendiboure, B. Simultaneous Application of the Gradient Theory and Monte Carlo Molecular Simulation for the Investigation of Methane/Water Interfacial Properties. *J. Phys. Chem. B* **2011**, *115*, 9618–9625.
- (37) Neyt, J. C.; Wender, A.; Lachet, V.; Malfreyt, P. Modeling the Pressure Dependence of Acid Gas + n-Alkane Modeling the pressure

dependence of acid gas + n-alkane Interfacial tensions using atomistic Monte Carlo simulations. *J. Phys. Chem. C* **2012**, *116*, 10563–10572.

(38) Neyt, J. C.; Wender, A.; Lachet, V.; Ghoufi, A.; Malfreyt, P. Molecular modeling of the liquid-vapor interfaces of a multi-component mixture: Prediction of the coexisting densities and surface tensions at different pressures and gas compositions. *J. Chem. Phys.* **2013**, *139*, 024701.

(39) Fernandes, P. A.; Cordeiro, M. N. D. S.; Gomes, J. A. N. F. Molecular Dynamics Simulation of the Water 2-Heptanone Liquid-Liquid Interface. *J. Phys. Chem. B* **1999**, *103*, 6290–6299.

(40) Cordeiro, M. N. D. S. Interfacial Tension Behaviour of Water/Hydrocarbon Liquid-Liquid Interfaces: A Molecular Dynamics Simulation. *Mol. Simul.* **2003**, *29*, 817–827.

(41) Patel, A.; Nauman, E. B.; Garde, S. Molecular structure and hydrophobic solvation thermodynamics at an octane–water interface. *J. Chem. Phys.* **2003**, *119*, 9199–9206.

(42) Li, Z.; Cranston, B.; Zhao, L.; Choi, P. Molecular Dynamics Studies of the Stability of Water/n-Heptane Interfaces with Adsorbed Naphthenic Acids. *J. Phys. Chem. B* **2005**, *109*, 20929–20937.

(43) Beierlein, F. R.; Krause, A. M.; Jager, C. M.; Fita, P.; Vauthey, E.; Clark, T. Molecular Dynamics Simulations of Liquid Phase Interfaces: Understanding the Structure of the Glycerol/Water-Dodecane System. *Langmuir* **2013**, *29*, 11898–11907.

(44) Zhang, Y.; Feller, S. E.; Brooks, B. R.; Pastor, R. W. Computer simulation of liquid/liquid interfaces. I. Theory and application to octane/water. *J. Chem. Phys.* **1995**, *23*, 10252–10266.

(45) van Buuren, A. R.; Marrink, S. J.; Berendsen, H. J. C. A Molecular Dynamics Study of the Decane/Water Interface. *J. Phys. Chem.* **1993**, *97*, 9206–9212.

(46) Rivera, J. L.; McCabe, C.; Cummings, P. T. Molecular simulations of liquid-liquid interfacial properties: Water–n-alkane and water-methanol–n-alkane systems. *Phys. Rev. E* **2003**, *67*, 011603.

(47) Jang, S. S.; Lin, S. T.; Maiti, P. K.; Blanco, M.; A, G., III; Shuler, P.; Tang, Y. Molecular Dynamics Study of a Surfactant-Mediated Decane-Water Interface: Effect of Molecular Architecture of Alkyl Benzene Sulfonate. *J. Phys. Chem. B* **2004**, *108*, 12130–12140.

(48) de Lara, L. S.; Michelon, M. F.; Miranda, C. R. Molecular Dynamics Studies of Fluid/Oil Interfaces for Improved Oil Recovery Processes. *J. Phys. Chem. B* **2012**, *116*, 14667–14676.

(49) Vazdar, M.; Pluharova, E.; Mason, P. E.; Vacha, R.; Jungwirth, P. Ions at Hydrophobic Aqueous Interfaces: Molecular Dynamics with Effective Polarization. *J. Phys. Chem. Lett.* **2012**, *3*, 2087–2091.

(50) Nickerson, S.; Frost, D. S.; Phelan, H.; Dai, L. L. Comparison of the Capillary Wave Method and Pressure Tensor Route for Calculation of Interfacial Tension in Molecular Dynamics Simulations. *J. Comput. Chem.* **2013**, *34*, 2707–2715.

(51) Cai, B. Y.; Yang, J. T.; Guo, T. M. Interfacial Tension of Hydrocarbon + Water/Brine Systems under High Pressure. *J. Chem. Eng. Data* **1996**, *41*, 493–496.

(52) Goebel, A.; Lunkenheimer, K. Interfacial Tension of the Water/n-Alkane Interface. *Langmuir* **1997**, *13*, 369–372.

(53) Zeppieri, S.; Rodriguez, J.; de Ramos, A. L. L. Interfacial Tension of Alkane + Water Systems. *J. Chem. Eng. Data* **2001**, *46*, 1086–1088.

(54) Bahramian, A.; Danesh, A. Prediction of liquid-liquid interfacial tension in multi-component systems. *Fluid Phase Equilib.* **2004**, *221*, 197–205.

(55) Hampton, P.; Darde, T.; James, R.; Wines, T. H. Liquid-liquid separation technology. *Oil Gas J.* **2001**, *99*, 54–57.

(56) Demond, A. H.; Lindner, A. S. Estimation of Interfacial Tension between Organic Liquids and Water. *Environ. Sci. Technol.* **1993**, *27*, 2318–2331.

(57) Marrink, S. J.; de Vries, A. H.; Mark, A. E. Coarse Grained Model for Semiquantitative Lipid Simulations. *J. Phys. Chem. B* **2004**, *108*, 750–760.

(58) Marrink, S. J.; Risselada, H. J.; Yefimov, S.; Tieleman, D. P.; de Vries, A. H. The MARTINI Force Field: Coarse Grained Model for Biomolecular Simulations. *J. Phys. Chem. B* **2007**, *111*, 7812–7824.

(59) Mayoral, E.; Nahmad-Achar, E. Study of interfacial tension between an organic solvent and aqueous electrolyte solutions using electrostatic dissipative particle dynamics simulations. *J. Chem. Phys.* **2012**, *137*, 194701.

(60) Leontyev, I.; Stuchebrukhov, A. Electronic continuum model for molecular dynamics simulations. *J. Chem. Phys.* **2009**, *130*, 085102.

(61) Leontyev, I.; Stuchebrukhov, A. Accounting for electronic polarization in non-polarizable force fields. *Phys. Chem. Chem. Phys.* **2011**, *13*, 2613–2626.

(62) Neyt, J. C.; Wender, A.; Lachet, V.; Szymczyk, A.; Ghoufi, A.; Malfreyt, P. How does the electronic continuum model perform in the prediction of the surface tension of salt solutions? *Chem. Phys. Lett.* **2014**, *595–596*, 209–213.

(63) Martin, M. G.; Siepmann, J. I. Transferable potentials for phase equilibria. 1. United-atom description of n-alkanes. *J. Phys. Chem. B* **1998**, *102*, 2569–2577.

(64) Chen, B.; Potoff, J.; Siepmann, J. I. Monte Carlo Calculations for Alcohols and Their Mixtures with Alkanes. Transferable Potentials for Phase Equilibria 5. United-Atom Description of Primary, Secondary and Tertiary Alcohols. *J. Phys. Chem. B* **2001**, *105*, 3093–3104.

(65) Abascal, J. L. F.; Vega, C. A general purpose model for the condensed phases of water: TIP4P/2005. *J. Chem. Phys.* **2005**, *123*, 234505.

(66) Chandrasekhar, J.; Spellmeyer, D. C.; Jorgensen, W. L. Energy component analysis for dilute aqueous solutions of lithium(1+), sodium(1+), fluoride(1-), and chloride(1-) ions. *J. Am. Chem. Soc.* **1984**, *106*, 903–910.

(67) D'Auria, R.; Tobias, D. J. On the relation between surface tension and ion adsorption at the air-water interface: a molecular dynamics simulation study. *J. Phys. Chem. A* **2009**, *113*, 7286–7293.

(68) Jorgensen, W. L.; Tirado-Rives, J. The OPLS Force Field for Proteins. Energy Minimizations for Crystals of Cyclic Peptides and Crambin. *J. Am. Chem. Soc.* **1988**, *110*, 1657–1666.

(69) Jorgensen, W.; Maxwell, D. S.; Tirado-Rives, J. Development and Testing of the OPLS All-Atom Force Field on Conformational Energetics and Properties of Organic Liquids. *J. Am. Chem. Soc.* **1996**, *118*, 11225–11236.

(70) Neyt, J. C.; Wender, A.; Lachet, V.; Ghoufi, A.; Malfreyt, P. Prediction of the concentration dependence of the surface tension and density of salt solutions: atomistic simulations using Drude oscillator polarizable and nonpolarizable models. *Phys. Chem. Chem. Phys.* **2013**, *15*, 11679.

(71) Wick, C. D.; Martin, M. G.; Siepmann, J. I. Transferable potentials for phase equilibria. 4. United-Atom description of linear and branched alkenes and alkylbenzenes. *J. Phys. Chem. B* **2000**, *104*, 8008–8016.

(72) Allen, M. P.; Tildesley, D. J. In *Computer Simulations of Liquids*; Press, O. U., Ed.; Clarendon Press: Oxford, U. K., 1989.

(73) Smith, E. R. Electrostatic Energy in Ionic Crystals. *Proc. R. Soc. London, Ser. A* **1981**, *375*, 475–505.

(74) Heyes, D. M. Pressure tensor of partial-charge and point-dipole lattices with bulk and surface geometries. *Phys. Rev. B* **1994**, *49*, 755–764.

(75) Ibergay, C.; Malfreyt, P.; Tildesley, D. J. Electrostatic Interactions in Dissipative Particle Dynamics: Toward a Mesoscale Modeling of the Polyelectrolyte Brushes. *J. Chem. Theory Comput.* **2009**, *5*, 3245–3259.

(76) Maurel, G.; Schnell, B.; Goujon, F.; Couty, M.; Malfreyt, P. Multiscale Modeling Approach toward the Prediction of Viscoelastic Properties of Polymers. *J. Chem. Theory Comput.* **2012**, *8*, 4570–4579.

(77) Yesylevskyy, S. O.; Schäfer, L. V.; Sengupta, D.; Marrink, S. J. Polarizable Water Model for the Coarse-Grained MARTINI Force Field. *PLoS Comp. Biol.* **2010**, *6*, 1–17.

(78) Sergi, D.; Scocchi, G.; Ortona, A. Coarse-graining MARTINI model for molecular-dynamics simulations of the wetting properties of graphitic surfaces with non-ionic, long-chain, and T-shaped surfactants. *J. Chem. Phys.* **2012**, *137*, 094904.

- (79) Winger, M.; Trzesniak, D.; Baron, R.; van Gunsteren, W. F. Comment on "On using a too large integration time step in molecular dynamics simulations of coarse-grained molecular models. *Phys. Chem. Chem. Phys.* **2010**, *12*, 2254–2256.
- (80) Badyal, Y. S.; Saboungi, M.-L.; Price, D. L.; Shastri, S. D.; Haeflner, D. R.; Soper, A. K. Electron distribution in water. *J. Chem. Phys.* **2000**, *112*, 9206–9208.
- (81) Rowlinson, J. S.; Widom, B. *Molecular Theory of Capillarity*; Clarendon Press: Oxford, U. K., 1982.
- (82) Kirkwood, J. G.; Buff, F. P. The Statistical Mechanical Theory of Surface Tension. *J. Chem. Phys.* **1949**, *17*, 338.
- (83) Irving, J. H.; Kirkwood, J. G. The Statistical Mechanical Theory of Transport Processes. IV. The Equations of Hydrodynamics. *J. Chem. Phys.* **1950**, *18*, 817–829.
- (84) Walton, J. P. R. B.; Tildesley, D. J.; Rowlinson, J. S.; Henderson, J. R. The pressure tensor at the planar surface of a liquid. *Mol. Phys.* **1983**, *48*, 1357–1368.
- (85) Walton, J. P. R. B.; Gubbins, K. E. The pressure tensor in an inhomogeneous fluid of non-spherical molecules. *Mol. Phys.* **1986**, *58*, 679–688.
- (86) Guo, M.; Lu, B. C. Y. Long range corrections to mixture properties of inhomogeneous systems. *J. Chem. Phys.* **1998**, *109*, 1134.
- (87) Ghoufi, A.; Malfreyt, P. Entropy and enthalpy calculations from perturbation and integration thermodynamics methods using molecular dynamics simulations: applications to the calculation of hydration and association thermodynamic properties. *Mol. Phys.* **2006**, *104*, 2929–2943.
- (88) Ladd, A. J. C.; Woodcock, L. V. Interfacial and coexistence properties of the Lennard-Jones system at the triple point. *Mol. Phys.* **1978**, *36*, 611–619.
- (89) Berendsen, H. J. C.; Postma, J. P. M.; van Gunsteren, W.; DiNola, A.; Haak, J. R. Molecular-Dynamics with Coupling to an External Bath. *J. Chem. Phys.* **1984**, *81*, 3684–3690.
- (90) DL_POLY is a parallel molecular dynamics simulation package developed at the Daresbury Laboratory Project for Computer Simulations under the auspices of the EPSRC for the Collaborative Computational Project for Computer Simulation of Condensed phases (CCPS) and the Advanced Research Computing Group (ARCG) at the Daresbury Laboratory.
- (91) Lemmon, E. W.; McLinden, M. O.; Friend, D. G. In *Thermophysical Properties of Fluid Systems*; Linstrom, P. J., Mallard, W. G., Eds.; National Institute of Standards and Technology: Gaithersburg, MD, 2005; NIST Chemistry Webbook, NIST Standard Reference Database Number 69. <http://webbook.nist.gov> (accessed on Jan. 13, 2014).
- (92) Baoukina, S.; Marrink, S. J.; Tieleman, D. P. Lateral pressure profiles in lipid monolayers. *Faraday Discuss.* **2010**, *144*, 393–409.
- (93) Carpenter, I. L.; Hehre, W. J. A Molecular Dynamics Study of the Hexane/water Interface. *J. Phys. Chem.* **1990**, *94*, 531–536.
- (94) Patel, S. A.; Brooks, C. L. Revisiting the hexane-water interface via molecular dynamics simulations using nonadditive alkane-water potentials. *J. Chem. Phys.* **2006**, *124*, 204706.
- (95) Malfreyt, P. Calculation of the surface tension of planar interfaces by molecular simulations: from Lennard-Jones fluids to binary mixtures. *Mol. Simul.* **2014**, *40*, 106–114.
- (96) Pegram, L. M.; Record, M. T.; Hofmeister, J. Salt Effects on Surface Tension Arise from Partitioning of Anions and Cations between Bulk Water and the Air-Water Interface. *J. Phys. Chem. B* **2007**, *111*, 5411–5417.